

Article

Impact of Copper Loading on NH₃-Selective Catalytic Reduction, Oxidation Reactions and N₂O Formation over Cu/SAPO-34

Kirsten Leistner ¹, Florian Brüsewitz ¹, Kurnia Wijayanti ¹, Ashok Kumar ²,
Krishna Kamasamudram ² and Louise Olsson ^{1,*}

¹ Competence Centre for Catalysis, Chemical Engineering, Chalmers University of Technology, SE-412 96 Gothenburg, Sweden; leistner@chalmers.se (K.L.); florianbruesewitz@gmx.net (F.B.); kurnia@chalmers.se (K.W.)

² Cummins Inc., 1900 McKinley Ave, MC 50183, Columbus, IN 47201, USA; kumar.a@cummins.com (A.K.); krishna.kamasamudram@cummins.com (K.K.)

* Correspondence: louise.olsson@chalmers.se; Tel.: +46-31-772-4390

Academic Editor: Evangelos G. Giakoumis

Received: 4 February 2017; Accepted: 22 March 2017; Published: 5 April 2017

Abstract: We developed a procedure for aqueous ion exchange to obtain different Cu loadings of Cu/SAPO-34 (between 0 and 2.6 wt %). The catalysts were washcoated on monoliths and characterised with respect to their activity and selectivity under standard selective catalytic reduction (SCR), fast SCR, NH₃ oxidation and NO oxidation reactions. They were further characterised using X-ray diffraction (XRD), Brunauer–Emmett–Teller (BET), H₂-temperature programmed reduction (H₂-TPR), ultraviolet (UV)-vis spectroscopy and NH₃ adsorption. As expected, activity of all reactions increased with copper loading, due to increased number of active sites. However, the N₂O formation during standard and fast SCR yielded interesting mechanistic information. We observed that N₂O formation at low temperature increased with copper loading for the standard SCR reaction, while it decreased for fast SCR. The low-temperature N₂O formation during fast SCR thus occurs predominantly over Brønsted sites. Species responsible for N₂O formation during standard SCR, on the other hand, are formed on the copper sites. We further found that the fast SCR reaction occurs to a significant extent even over the H/SAPO-34 form. The Brønsted sites in SAPO-34 are thus active for the fast SCR reaction.

Keywords: selective catalytic reduction (SCR); Cu/SAPO-34; copper loading; chabazite; fast SCR; ammonia oxidation; N₂O

1. Introduction

Continuous improvement of NO_x removal technologies is made possible by the development of increasingly efficient catalysts. Thus, ammonia-selective catalytic reduction (SCR) was initially widely catalysed by noble metals [1–3]. Vanadia-based catalysts then became common and later on, metal-exchanged zeolites [1,4–6]. Most recently, small-pore materials such as the zeolite Cu/SSZ-13 and the silicoaluminophosphate Cu/SAPO-34, have become popular subjects of research [7–9].

One aspect of Cu/SAPO-34 is the difficulty in producing it using conventional aqueous ion exchange [3,10]. Thus, a number of studies have been published on Cu/SAPO-34 synthesised via one-pot synthesis or solid state ion exchange and on commercially-produced catalysts [11,12]. However, very few details are available as to the procedure of aqueous ion exchange for Cu/SAPO-34.

Copper loading and copper ion exchange level are amongst the major properties to have an effect on the reduction of NO_x over Cu/zeolites. Thus, optimum deNO_x efficiency over a range of temperatures is usually obtained at an intermediate Cu content [13] due to its positive correlation

with both the SCR reaction and the competitive NH_3 oxidation reaction. Moreover, Cu site distribution has been found to vary with Cu loading on a number of different zeolites [14–17]. For instance, more cupric oxides are formed at higher copper loadings, especially on over-exchanged zeolites [18]. For Cu/SSZ-13, it was shown that copper ions occupy different positions within the crystal structure. At lower Cu contents, they are positioned at sites in the 6-membered rings and at higher contents, also within the large cages [19]. There are indications that Cu ions may be sited similarly in Cu/SAPO-34 [11].

In addition to its importance for SCR activity, copper loading may also yield useful information on the reaction selectivities and pathways, as we have previously shown for Cu/Beta [16]. For instance, different product gases may exhibit differing trends in function of copper content, thus providing evidence for the existence of different mechanisms or active sites. Such knowledge of the reaction mechanisms is essential for the development of kinetic models. While some investigations of the behaviour of Cu/SAPO-34 as a function of Cu loading have been published [20,21], there are still many mechanistic questions remaining. Furthermore, no kinetic models of SCR over Cu/SAPO-34 appear to have been published, so more mechanistic studies are of interest.

Hence, the main objective of this study is to characterize a series of Cu/SAPO-34 catalysts of different copper loadings with respect to the selectivities of a number of product gases and the reactions they occur in: standard SCR, fast SCR, NH_3 oxidation and NO oxidation. This data then allows us to draw conclusions pertaining to the reaction mechanisms, with a particular focus on the N_2O formation during standard and fast SCR. In addition, detailed synthesis information is provided, which allows for aqueous ion-exchange of the SAPO-34 material.

2. Results

2.1. Characterisation by X-ray Diffraction (XRD)

XRD diffractograms were acquired for all catalysts before and after aqueous ion exchange with NH_4NO_3 and $\text{Cu}(\text{NO}_3)_2$ solutions. The diffractograms for all copper-loaded catalysts are shown in Figure 1 together with that of one of the SAPO-34 batches.

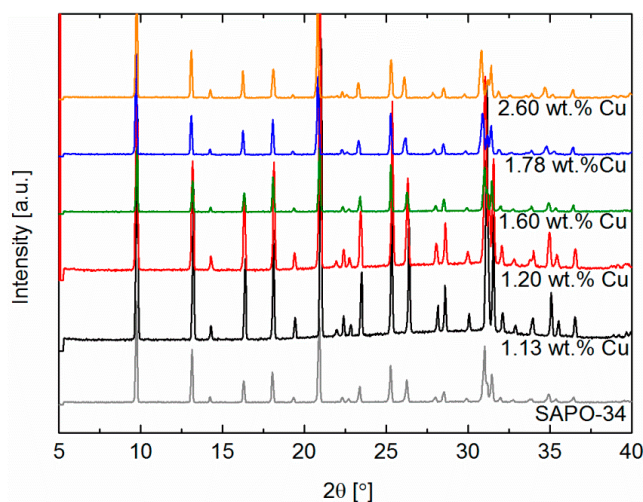


Figure 1. X-ray diffractograms (XRDs) of SAPO-34 and Cu/SAPO-34 with different Cu loadings.

Most diffractograms in Figure 1 are very similar to that of pure SAPO-34, indicating that the chabazite (CHA) structure was maintained during ion exchange. Cu_2O or CuO phases may be expected at ca. $2\theta = 35.29, 36.30, 38.49$ and 38.72° [20,22,23], but the diffractograms do not display any evidence of these species, presumably because the copper oxide content is relatively low and consists of isolated ions or because it is very well dispersed [22,23]. Wang et al. found that the diffraction peaks for ion-exchanged zeolites moved to slightly lower angles with respect to the unexchanged support, suggesting that the SAPO-34 lattice had expanded with incorporation of the Cu ions into

the pores. Here, a similar trend can be seen when comparing Cu/SAPO-34 1.60–2.60 wt % Cu with SAPO-34.

2.2. Characterisation by N₂ Adsorption

All catalysts were further characterized by nitrogen adsorption-desorption and the resulting Brunauer–Emmett–Teller (BET) surface areas and microporous volumes are shown in Table 1. While nitrogen adsorption cannot be used for a true quantitative assessment of microporosity in small-pore materials, it nevertheless allows for an empirical comparison of the different catalysts before and after ion exchange [24]. In the present study, only a small loss of BET surface areas was observed after ion exchange as compared to the parent SAPO-34 materials, and in some cases even an increase was observed. The accompanying change in microporous volume upon introduction of copper was also small, as may be seen in Table 1.

Table 1. Catalysts synthesised in this study. All catalysts are shown with the corresponding parent material (SAPO-34 batches not exchanged with NH₄NO₃ or Cu(NO₃)₂). BET: Brunauer–Emmett–Teller.

Batch	Type	Molarity Cu(NO ₃) ₂ Solution (M)	Cu wt %	Cu/Si (mol/mol)	Calcination Temperature (°C)	BET Surface Area (m ² /g)	Micropore Volume (cm ³ /g)
1	SAPO-34		0			530.0	0.243
	Cu/SAPO-34	0.6	1.78	0.15	750	551.1	0.257
	Cu/SAPO-34	0.4	1.49	0.12	550	622.3	0.290
2	SAPO-34		0			570.6	0.265
	H/SAPO-34		0		750	513.9	0.237
	Cu/SAPO-34	0.4	1.60	0.15	750	588.2	0.277
3	SAPO-34		0			587.8	0.294
	Cu/SAPO-34	0.8	2.60	0.20	750	544.2	0.255
4	SAPO-34		0			574.5	0.284
	Cu/SAPO-34	0.05	1.13	0.11	750	568.9	0.282
	Cu/SAPO-34	0.2	1.20	0.11	750	536.6	0.253
5	SAPO-34		0			584.2	0.289
	Cu/SAPO-34	0.2	1.27	0.12	550	581.9	0.274

2.3. Catalyst Composition and Copper Species

Catalyst composition was determined by inductively-coupled plasma sector field mass spectrometry (ICP-SFMS) and the resulting copper loadings are shown in Table 1. Na and Fe contamination is negligible, where the Na and Fe amounts are below the detection limit of 0.04 and 0.07 wt % respectively for all catalysts. The (Si + P)/Al ratios of all catalysts are comprised between 0.90 and 1.02. In this study, copper loadings range between 1.13 and 2.60 wt %. For Cu/Beta zeolites, Mihai et al. reported a progressive decrease of surface area with increasing copper content, attributed to greater numbers of blocked pores in the samples with higher Cu loading [16]. No particular trend regarding the BET area with respect to Cu loading is noticed for the Cu/SAPO-34 catalysts in this study. This could possibly be due to the fact that the parent SAPO-34 were different batches. Cu/Si ratios are also given in Table 1, and levels of ion exchange are calculated and shown in Table S1 in the Supplementary Materials. They range between 21.2 and 39.1%, which means that none of the samples are over-exchanged.

In order to characterize the Cu species, ultraviolet (UV)-vis diffuse reflectance (DR) spectra of the catalysts were acquired, and the results are shown in Figure 2a. Several studies have assigned the charge transfer band at around 225 nm to the O_(SAPO-34) → Cu⁺/Cu²⁺ charge transition [25–27]. A broad band centred at around 800 nm has been assigned to the d → d transition of isolated Cu²⁺, and also coincides with the bands observed in the reference material Cu(OH)₂ [25–28]. This band, representative of isolated, hydrated Cu(II), has been identified on a number of copper-exchanged zeolites, including Cu/BEA, Cu/ZSM-5 and Cu/SSZ-13 [29–31]. At around 1420 nm, a third band is observed. All the Cu/SAPO-34 catalysts in this study display these three major bands, with the exception of H/SAPO-34, which does not have the Cu(II) band at 800 nm. Thus, the bands at low and

high wavelengths are not only due to the copper species but also originate from the SAPO-34 framework, whereas bands at intermediate wave lengths are characteristic of copper species. In the literature, two bands at 355 and 456 nm have been attributed to oxidic copper complexes on Cu/SAPO-34 catalysts [27]. In Figure 2a the two bands cannot be distinguished, but the broad band between 350 and 550 nm is possibly a convolution of the two contributions. Furthermore, we previously found a broad, flat peak from the low wavelengths up to about 800 nm, for both reference CuO bulk material and severely hydrothermally-aged Cu/BEA samples [31]. H₂-temperature programmed reduction (H₂-TPR) of the three samples with highest Cu loading was also performed (Figure S1), and resulted in a single H₂ consumption peak. This indicates that all of the copper ions were located in the identical ion exchange positions, presumably the 6-membered rings, since higher copper loadings are necessary for the ions to be located in the large cages [19].

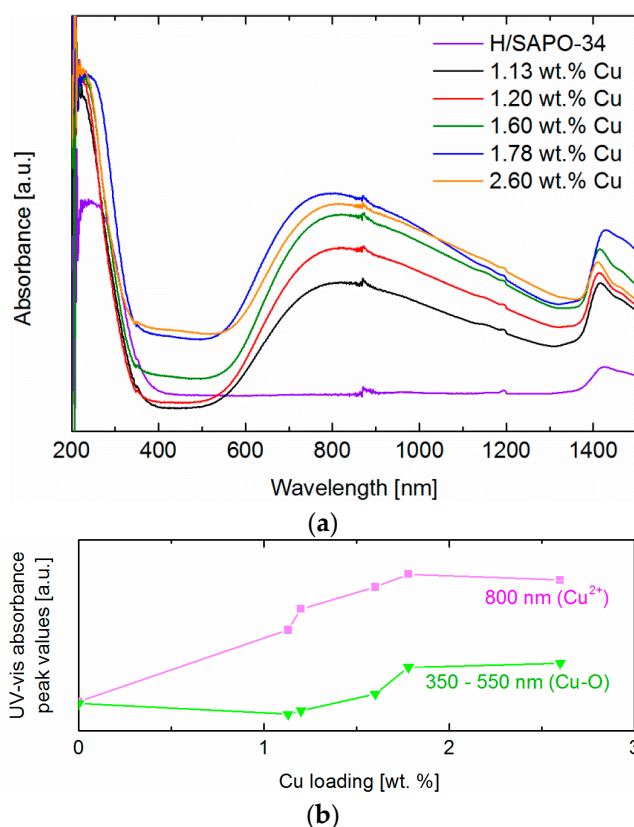


Figure 2. UV-vis data for Cu/SAPO-34 catalysts. (a) UV-vis spectra of Cu/SAPO-34 catalysts with different Cu loadings; (b) UV-vis absorbance band intensities as a function of Cu loading.

As far as the trend with copper concentration during ion exchange is concerned, peak heights from Figure 2a were plotted as a function of copper loading in Figure 2b. Note that the y-axis shows peak height values read off Figure 2a, not peak areas from deconvolution. We made a choice not to deconvolute the peaks because features were very broad, so that several different fits would have been possible. It must be emphasised here that the UV-vis spectra and peak heights should be interpreted qualitatively. Figure 2b suggests that the intensity of both Cu(II) and oxidic copper bands overall increases with copper loading, although it (especially that of Cu(II)) levels off at a copper loading of 2.60 wt %. While this could indicate that there are fewer Cu(II) and Cu-O species than expected in the sample with the highest Cu loading, it should be kept in mind that quantitative interpretation of DR UV-vis measurements can be challenging, especially when no deconvolution is performed. Nevertheless, one possible reason for the levelling-off could be that high molarity during ion exchange results in large oxidic copper particles on the outside of the SAPO-34-particles. Indeed, formation of larger CuO clusters on the external zeolite surface is known to occur at higher copper loadings [20,21]. If the clusters are sufficiently large, Cu(II) and Cu-O type species in these particles might not all be detectable by the DR UV-vis technique above, which would explain the levelling off

of the Cu(II) and oxidic Cu bands [32]. We did in fact spot some large, Cu-containing particles during transmission electron microscopy + energy-dispersive X-ray spectroscopy (TEM + EDS) analysis (results shown in Figure S2), although without examining statistically significant numbers of SAPO-34 particles, the number of oxidic Cu particles found was not sufficient to be conclusive. Further, these interpretations must remain speculative since the UV-vis spectra do not yield quantitative information.

2.4. Characterisation by NH_3 Adsorption

Ammonia adsorption was used to study the storage capacity of the catalysts. The procedure consisted of a 2-h exposure to a feed of ammonia and water (5%) at 150 °C, after which the ammonia feed was cut off and the catalyst surface purged for 45 min, still at 150 °C and under 5% H_2O . Then, the temperature was ramped up to 500 °C at a rate of 10 °C /min under Ar and 5% H_2O . The desorption profiles are shown in Figure 3.

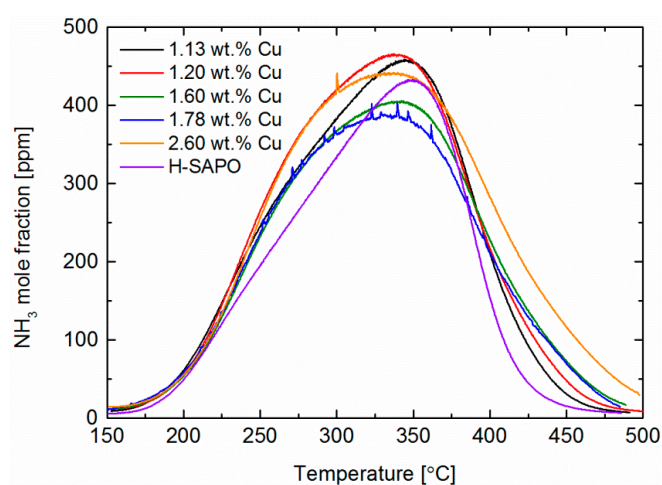


Figure 3. Temperature-programmed desorption (TPD) at 10 °C/min after storage of 400 ppm NH_3 at 150 °C and purge at 150 °C.

Ammonia molecules physisorbed onto weak Brønsted and Lewis acid sites and desorbed during the purge at 150 °C (not shown here) [20,33,34]. Integration of the signal for H/SAPO-34, yields a storage capacity of 0.59 mmol $\text{NH}_3/\text{g}_{\text{cat}}$. Given that the Si content of this sample is much larger, at 1.75 mmol Si/ g_{cat} , it is likely that H/SAPO-34 contains silicon islands [33,35,36]. The high-temperature desorption peak centred on average at about 340 °C can be attributed to strongly-bound NH_3 molecules adsorbed on both strong Brønsted sites and new Lewis acid sites generated by the incorporation of copper [33,34]. The asymmetric shape of the temperature-programmed desorption (TPD) profile indicates that there may be another, lower peak centred at around 250 °C. Such a peak has indeed been observed when adsorbing at temperatures lower than the 150 °C used here [20,33,34]. It has been assigned to desorption from either weak Brønsted sites or weak Lewis sites. The trend of total desorbed NH_3 in function of copper loading is increasing overall, but should be interpreted qualitatively, due to the fact that the catalysts stem from different parent batches, which may impact on the structure and the Si content of the SAPO-34 (see Table S1), and thus on the amounts adsorbed [33]. Furthermore, the interpretation of ammonia storage trends is made difficult by the fact that the number of Brønsted acid sites in zeolites decreases with the incorporation of copper, as Lewis acid sites are formed instead [20,37]. Thus, one cannot expect the relationship between copper loading and the area under the 250 and 340 °C peaks to be completely straightforward, as it would depend on the interplay between increasing numbers of Lewis sites and decreasing numbers of Brønsted sites. Nevertheless, and though the lower-temperature peak is present only as a shoulder, it seems that this shoulder increases with copper loading for most of the samples, supporting the assignment to weak Lewis sites. The shoulder is however also visible for H/SAPO-34, which indicates that ammonia stored on weak Brønsted sites also contributes to this desorption peak. Interestingly, with

increasing copper loading, we observe an increasing high temperature shoulder (400–500 °C) on the NH_3 -TPD curve, which is consistent with our previous findings for Cu/BEA [16]. It suggests that the increasing formation of copper oxide species with increasing copper loading, as indicated by UV-vis (Figure 2), may result in more strongly bound ammonia. In addition, the loosely bound ammonia desorbed at 150 °C (not shown here) also increases with copper loading, which was also the case for Cu/BEA [16].

2.5. NH_3 and NO Oxidation

The ammonia oxidation reaction commonly occurs under SCR conditions, thereby affecting the SCR reaction itself. Thus, we first investigated the impact of copper loading on this reaction and also on NO oxidation, before going on to study the effect on the standard and fast SCR reactions in the following sections. Ammonia oxidation experiments were performed on Cu/SAPO-34 with different Cu loadings. The feed contained 400 ppm of NH_3 , 8% O_2 and 5% H_2O . Figure 4 shows the steady state ammonia conversions for the different copper loadings. Ammonia oxidation becomes active at roughly 300 °C, depending on the copper content. For the two catalysts containing 1.78 and 2.60 wt % Cu, the 400 ppm of feed ammonia are almost completely oxidized at 600 °C.

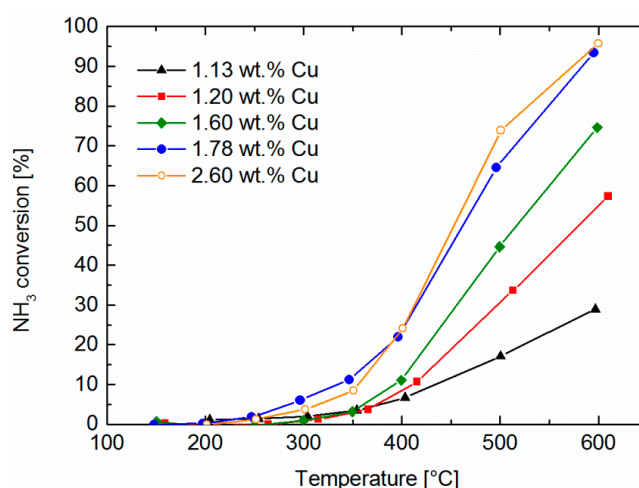


Figure 4. NH_3 conversion during NH_3 oxidation. Inlet: 400 ppm NH_3 , 8% O_2 , 5% H_2O .

NH_3 conversion clearly increases monotonically with copper loading, a trend that has also been observed for solid-state ion exchanged Cu/SAPO-34 [20]. It is worth noting, however, that between 1.78 and 2.60 wt % Cu, the NH_3 consumption increases quite little relative to the increase in Cu loading. This is in line with the comparably smaller increase in Cu-O-type species seen by UV-vis at this copper loading. The main product of the ammonia oxidation reaction occurring on Cu/SAPO-34 was found to be N_2 , with selectivities close to 100%. Only small amounts of side products are formed, with NO, NO_2 and N_2O not exceeding eight, two and three ppm, respectively. The side product selectivities found by Yu et al. for copper loadings of around 0.90 wt % are higher compared to ours, with maximum NO mole fractions ranging between 22 and 46 ppm depending on Si content [34]. Wang et al. find comparably little formation of side products [20], which is in line with our study.

NO oxidation experiments were conducted in conditions similar to the NH_3 oxidation experiments, the resulting NO_2 production is shown in Figure 5. As has been observed for small-pore zeolites, this reaction over Cu/SAPO-34 produces very little NO_2 , with a maximum under 6% [38,39]. The trend with copper loading is similar to that seen with NH_3 oxidation: increasing up to 1.78 wt % Cu with little increase thereafter.

2.6. Standard SCR

Standard SCR experiments were performed on Cu/SAPO-34 with different Cu loadings and H/SAPO-34. The feed contained 400 ppm NO, 400 ppm NH_3 , 8% O_2 and 5% H_2O . Resulting NO_x and

NH₃ conversions are shown in Figure 6a,b, respectively. As is also usual for small-pore zeolites, the SCR activity of Cu/SAPO-34 is higher over a wide temperature range, compared to other common Cu-zeolites [26,27,38]. At around 350 °C, the NO_x conversion starts to decrease while the NH₃ conversion is 100%. This behaviour is commonly seen over Cu-zeolites and is attributed to the competitive consumption of ammonia by the NH₃ oxidation reaction.

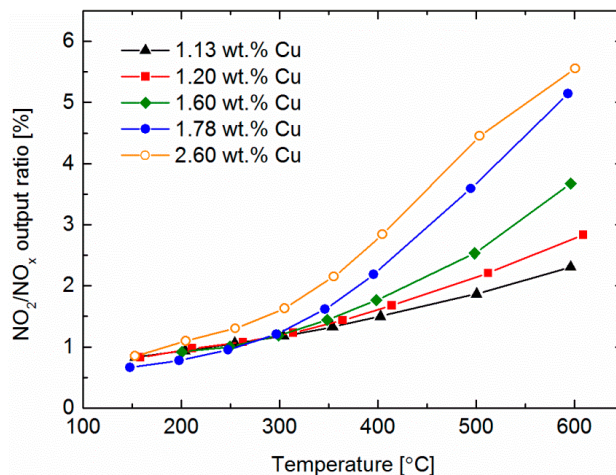
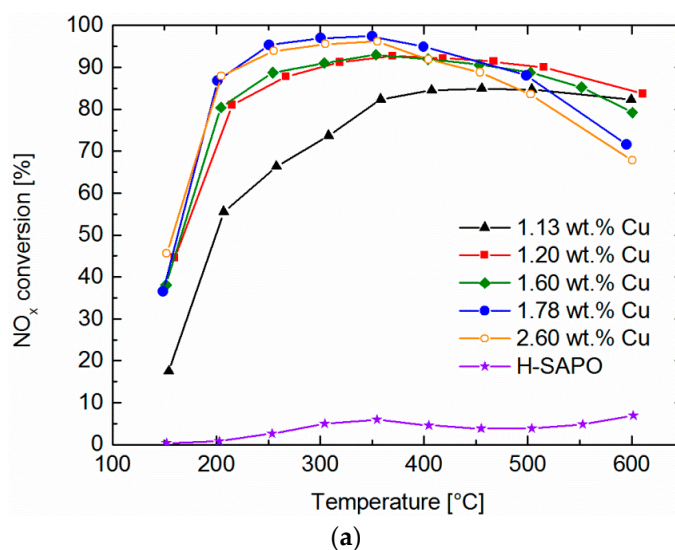


Figure 5. NO₂ formation during NO oxidation. Inlet: 400 ppm NO, 8% O₂, 5% H₂O.

Both NO_x and NH₃ conversion are considerably lower over H/SAPO-34 than over the copper-containing samples: the values do not exceed 6 and 12 %, respectively. This is consistent with what is usually seen for the H-form of zeolites. For example, Wang et al. found a maximum NO_x conversion of 14% for H/SAPO-34 [20] and similarly low activity has been observed with H/ZSM-5 [40]. Clearly the Cu sites therefore play an important role not only for NH₃ adsorption, as shown in Section 2.4, but even more so for the SCR reaction.



(a)

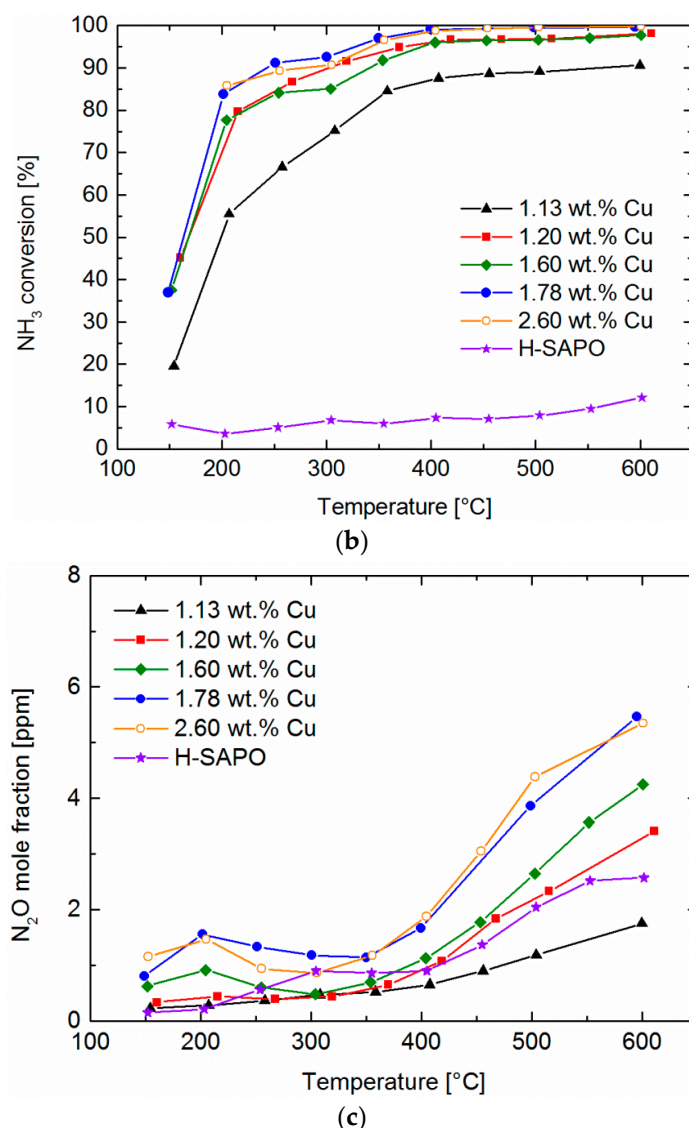


Figure 6. Standard selective catalytic reduction (SCR) steady state activity. Inlet: 400 ppm of NH₃, 400 ppm of NO, 8% O₂, 5% H₂O. (a) NO conversion; (b) NH₃ conversion; (c) N₂O production.

The relationship between copper loading, temperature and NO_x conversion follows two different trends depending on the temperature. The difference between the two trends has been highlighted by replotting the data of Figure 6a in function of Cu loading in Figure 7a. Note that the data pertaining to 1.20 wt % Cu has been left out because the catalyst temperatures differed from the gas phase values (200, 250, 300, 350, 400, 500 and 600 °C in Figure 7) by more than 8 °C. The top panel of Figure 7a shows that NO_x conversion increases with copper loading at temperatures below 350 °C. At higher temperatures (350–600 °C), the trend is inverted (at Cu loading above 1.13 wt %) and NO conversion decreases with copper content (at the higher temperatures) and with temperature, as may be seen in the bottom panel of Figure 7a. Our NH₃ oxidation experiments showed that the NH₃ oxidation reaction becomes active at around 350 °C and competes for NH₃ with the SCR reaction. Since NH₃ oxidation activity increases monotonically with Cu content (Figure 7b), the SCR activity of the materials with higher copper loadings is compromised more. As already mentioned in the previous section, NH₃ oxidation performance levels off for the highest copper loading, and this can possibly be attributed to the unexpectedly small amounts of Cu-O type species observed by DR UV-vis.

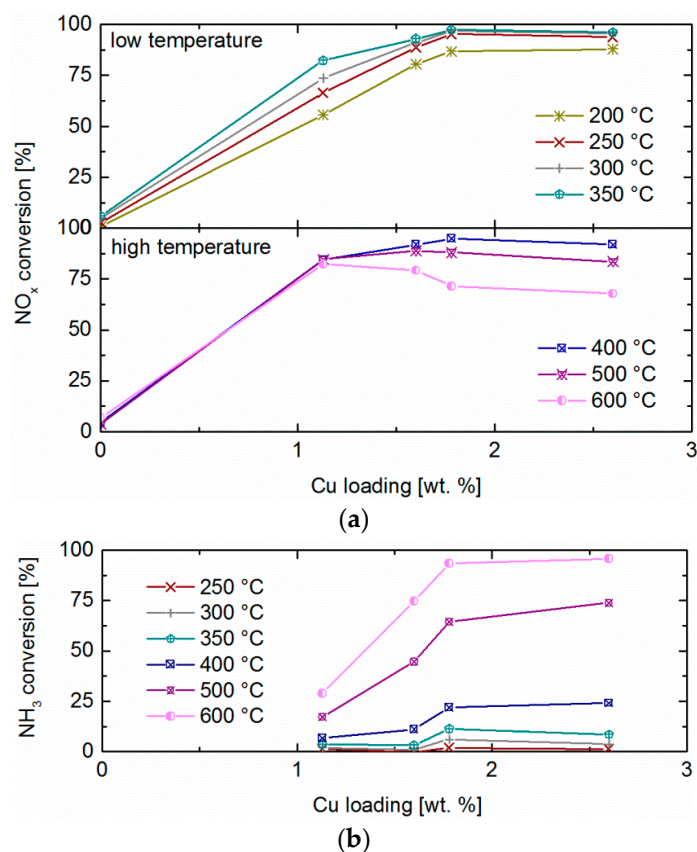


Figure 7. Steady state conversions in function of Cu loading. (a) NO_x conversion during SCR; (b) NH₃ conversion during NH₃ oxidation.

During the SCR experiments, small amounts of the side products N₂O and NO₂ were also detected in the outlet, and N₂O is shown in Figure 6c. The amounts of both are small (<6 ppm) compared to medium and large pore Cu-zeolites [21,38]. Like the NO_x conversion, both NO₂ and N₂O production exhibit an overall increase with increasing copper loading. Two maxima of N₂O production are observed, at ca. 200 and 600 °C. We have previously shown that Cu/SSZ-13 and Cu/Beta catalysts also produced two N₂O maxima during standard SCR [16,38,41]. This has led to the proposal that two different sites or reaction pathways are involved in the formation of N₂O [38], where precursors for ammonium nitrates such as NO-NH₃ species are suggested to be responsible for the low-temperature N₂O production [42].

2.7. Fast SCR

The selective catalytic reduction of NO_x in presence of equimolar amounts of NO and NO₂, is known as fast SCR and is much faster than the standard SCR with NO only [43]. The experiments in this section were carried out in identical conditions to the standard SCR experiments, except for the NO and NO₂ concentrations: 200 ppm NO, 200 ppm NO₂, 400 ppm NH₃, 8% O₂ and 5% H₂O in argon. Figure 8a,b show the obtained NO_x and NH₃ conversions, respectively. Note that the conversion is taken at the end of each temperature step and that steady state was not always reached at temperatures below 300 °C. This can be seen in Figure 9a, which shows the transient outlet NO_x during fast SCR. At 150 °C, the NO_x concentration exhibits a minimum, a behaviour that is known to be caused by the formation of ammonium nitrate species on the catalyst surface [38]. The formation of such species on Cu-zeolites is commonly attributed to the surface reaction of gaseous NH₃ with surface nitrates previously formed on copper sites.

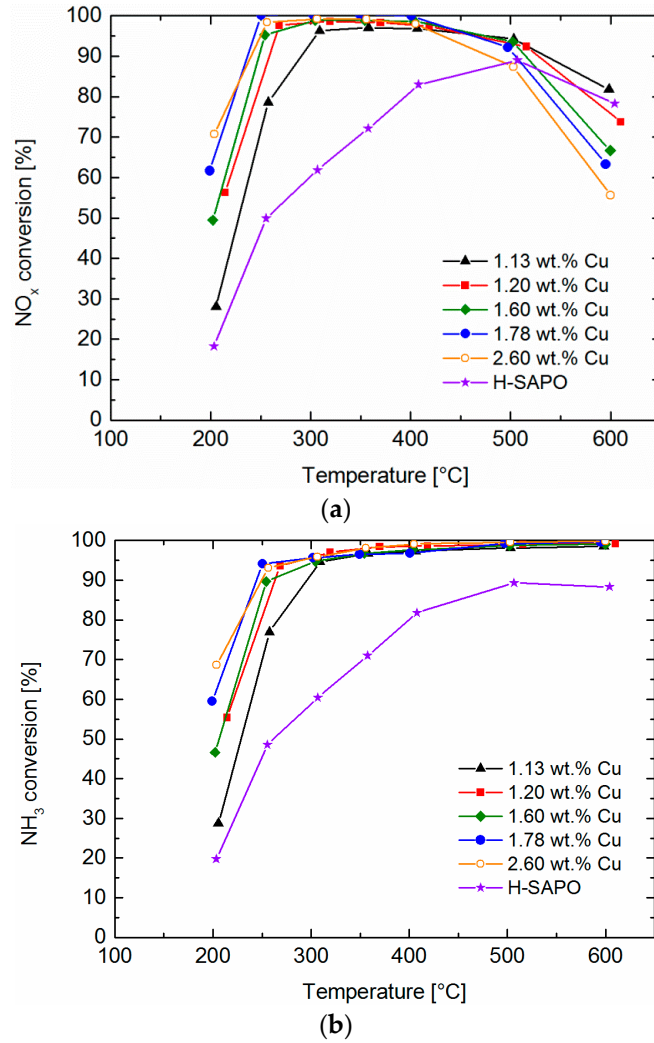
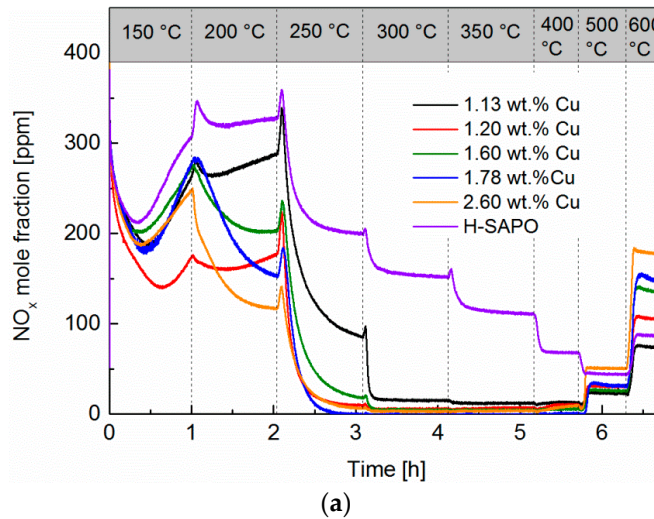


Figure 8. Fast SCR steady state activity. Inlet: 400 ppm NH₃, 200 ppm NO, 200 ppm NO₂, 8% O₂, 5% H₂O. (a) NO conversion; (b) NH₃ conversion.



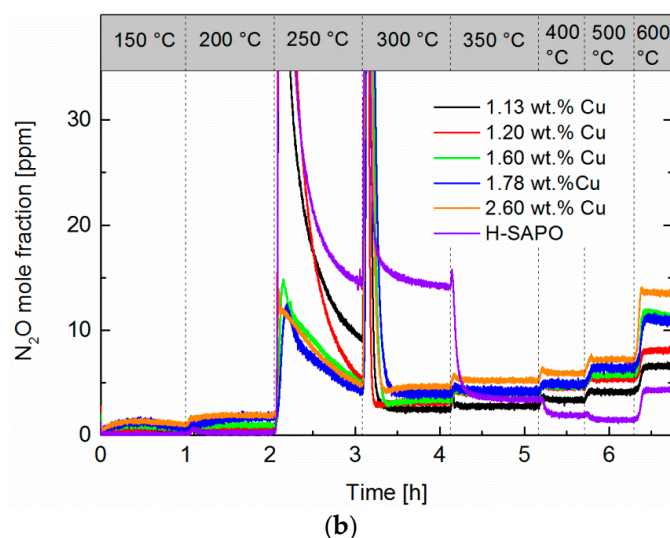


Figure 9. Fast SCR transient outlet NO_x (a) and N_2O (b). Inlet: 400 ppm NH_3 , 200 ppm NO , 200 ppm NO_2 , 8% O_2 , 5% H_2O .

Large N_2O concentrations during the temperature ramp between some of the temperature steps, such as those seen while heating to 250 and 300 °C (Figure 9b), can result from the decomposition of ammonium nitrate species [43,44]. At 300 °C and above, ammonium nitrate formation does not occur and steady state conditions are reached. Quantification of ammonium nitrates cannot be done by detecting the amount of N_2O at low temperature, since thermal decomposition of ammonium nitrate ($\text{NH}_4\text{NO}_3 = \text{N}_2\text{O} + 2\text{H}_2\text{O}$) is not the only path, as ammonium nitrate can react with NH_3 to form N_2 ($3\text{NH}_4\text{NO}_3 + 2\text{NH}_3 = 4\text{N}_2 + 9\text{H}_2\text{O}$). Only over H/SAPO-34 is it likely that ammonium nitrate decomposition entirely causes N_2O formation. The reason for this is that the $\text{N}_2\text{O}/\text{H}_2\text{O}$ yield ratio is below half with Cu/zeolites, and equal to half with H/zeolite, according to Gao et al. [45]. However, since the N_2O formation at low temperature is believed to originate from ammonium nitrate decomposition [43,44], the amount of N_2O is an indication of the amount of ammonium nitrates.

The relationship of low-temperature N_2O formation with Cu loading was quantified by integrating the amounts of N_2O released during the heating ramps to 250 and 300 °C. These calculated amounts are shown in function of copper loading in Figure 10. Surprisingly, the overall trend is decreasing susceptibility to N_2O formation with increasing Cu content. Over Cu/BEA it was clear that when increasing the copper loading, the N_2O formation increased also for fast SCR conditions [46]. Moreover, the N_2O formation over the copper-free H/SAPO-34 is significantly larger compared to the Cu-exchanged samples, where for example the H/SAPO-34 has about double amount of N_2O compared to Cu/SAPO-34 above 1.78 wt % Cu. We have shown in an earlier study that, in fast SCR conditions, Cu/SAPO-34 forms significantly less N_2O continuously, but that it deactivates much more severely due to ammonium nitrates compared to both Cu/SSZ-13 and Cu/BEA [38]. When these ammonium nitrates were decomposed, they resulted in huge N_2O formation over the Cu/SAPO-34 and it was suggested that the reason for the low continuous N_2O formation of Cu/SAPO-34 is that the ammonium nitrates formed are very stable and the decomposition is therefore slow, thereby lowering the continuous N_2O formation. However, when the ammonium nitrates were decomposed, large amounts of N_2O were seen [38].

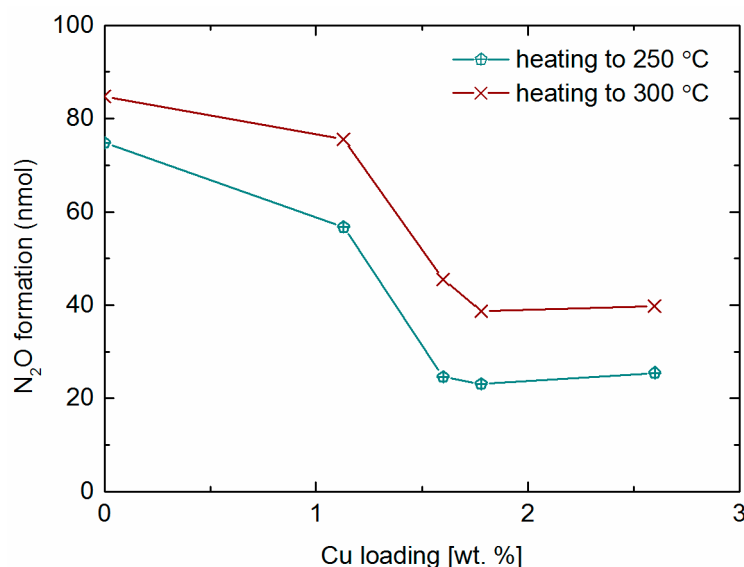


Figure 10. N₂O released while ramping from 200 to 250 °C and 250 to 300 °C during fast SCR.

The steady state data in Figure 8 shows that the fast SCR performance is inferior even to the standard SCR at low temperatures. This is caused by the formation of ammonium nitrate species lowering the number of accessible sites, thus inhibiting the SCR reaction. At intermediate temperatures (300–400 °C), highly-loaded samples convert more NO_x than samples with low Cu loading, although the difference is much smaller than during standard SCR. As for the standard SCR at high temperatures (above 400 °C), lack of reducing agent due to competitive ammonia oxidation causes a decrease of NO_x conversion with increasing copper loading. However, the decrease in NO_x conversion is much larger during fast SCR conditions compared to standard SCR; for example, for the 1.78 wt % Cu sample, the NO_x conversion is 72% at 600 °C for standard SCR, but only 63% for fast SCR. This could be caused by NO₂ reacting with NH₃ at high temperature to produce NO, which thereafter reacts in the standard SCR reaction [46]. This would result in larger ammonia consumption and thus, reduced NO_x conversion. Further, a comparison of Figures 6 and 8 shows that the difference between H/SAPO-34 and copper-loaded SAPO-34 is much more significant for the standard SCR reaction than the fast SCR reaction. NO_x conversion during standard SCR over H/SAPO-34 never exceeds 6%, whereas the maximum conversion obtained during fast SCR is 89%. Similarly, the beneficial effect of higher copper loadings is smaller during fast SCR compared to the standard SCR. These and similar observations over H/ZSM-5 [40,47,48] indicate that the fast SCR reaction is connected not only with copper sites, but also to a significant extent with the Brønsted acid sites.

2.8. Impact of Calcination Temperature

Two separate batches of SAPO-34 were exchanged with Cu(NO₃)₂ solutions of 0.4 M, to yield copper loadings of 1.49 and 1.60 wt %Cu. The former was calcined once at 550 °C, while the latter was also calcined a second time at 750 °C (according to the same procedure used for the other catalysts in this study). Figure 11 shows that both samples had comparable activities for the SCR and ammonia oxidation reactions below 450 °C. Above this temperature, the sample calcined at 750 °C was less active for ammonia oxidation (at 600 °C conversion was 75% as opposed to 89%) and more active for the SCR reaction (at 600 °C: 79% as opposed to 65%). Note that this sample has 0.11 wt % more copper than that calcined only once at 550 °C. While the greater SCR activity at high temperatures can be explained as a consequence of the smaller NH₃ oxidation ability and the slightly higher Cu loading, the smaller NH₃ conversion itself is not in line with our finding in Section 2.5 that NH₃ oxidation activity increases with increasing copper content. However, it can probably be attributed to the higher calcination temperature, given that CuO species are active for NH₃ oxidation (Section 2.5). It is likely that calcination at 750 °C causes oxidic copper species to move into the structure. This interpretation is consistent with findings that Cu ions migrate from the catalyst surface

into ion exchange positions in the SAPO-34 pores [28,42,49,50] (for example during solid-state ion-exchange) and with our observation that Cu/SAPO-34 1.49 and 1.60 wt % Cu are grey in colour after calcination at 550 °C and turn blue after the second calcination at 750 °C. UV-vis spectra were acquired for the two samples calcined at 550 and 750 °C and are shown in the top panel of Figure 12. The two spectra differ mainly in the region between 350 and 550 nm. Calcination at the higher temperature leads to lesser absorption at these wavelengths, which is indicative of a smaller number of Cu-O-type species. These findings thus further support the above interpretation that copper oxides move into ion-exchange positions, which decreases the ammonia oxidation and simultaneously increases the SCR activity. Interestingly, a different observation is made with the spectra of two catalysts with lower Cu loadings (bottom panel of Figure 12). Here, the effect of the calcination temperature on the presence of oxidic copper species is much less pronounced. In fact, the colour difference (grey after calcination at 550 °C and blue after calcination at 750 °C) was seen only for copper loadings above 1.49 wt % Cu. The high copper loadings were produced by increasing the molarity of the copper nitrate solution. Thus, we propose that the high $\text{Cu}(\text{NO}_3)_2$ concentration results in copper oxide particles on the outside, and that the copper in these particles is later moved into the structure during high temperature calcination. As discussed above, it is a possibility that for the highest copper nitrate concentration (0.8 M) some of these copper oxide particles remain, and that the copper therein is inactive for some of the reactions.

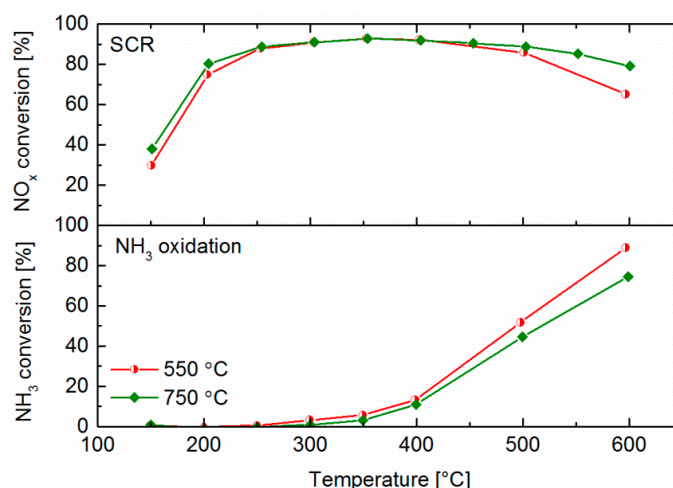


Figure 11. NO_x conversion during SCR (top panel) and NH_3 conversion during NH_3 oxidation (bottom panel) for Cu/SAPO-34 calcined at two different temperatures (550 and 750 °C). Cu contents: 1.49 and 1.60 wt %, respectively.

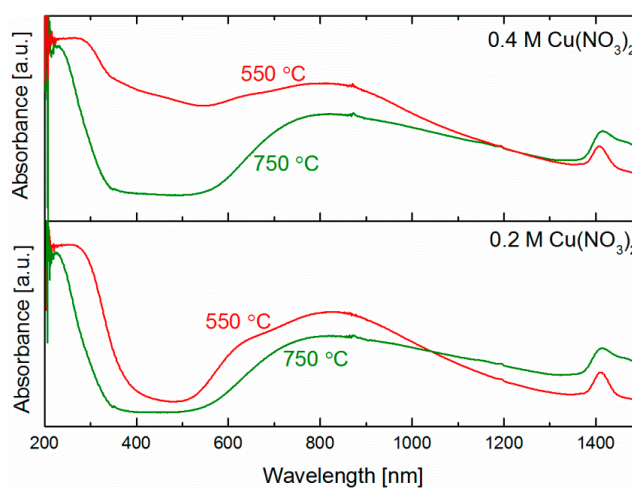


Figure 12. UV-vis spectra of Cu/SAPO-34 calcined at two different temperatures (550 and 750 °C). Top panel: 1.49 and 1.60 wt % Cu. Bottom panel: 1.27 and 1.20 wt % Cu.

3. Discussion

Different copper loadings in Cu/SAPO-34 were obtained by ion exchange with copper nitrate solutions of molarities ranging from 0.05 to 0.8 M. A clear trend was observed, with increasing copper loading resulting in higher SCR, fast SCR, and NH_3 and NO oxidation activity. This increasing trend levelled off for the highest copper loading. Not surprisingly, UV-vis results indicated that the number of Cu(II) and CuO species increased with copper loading. Note that this increase also levelled off at the highest copper loading, thus explaining the smaller increase in activity for this sample. Despite the formation of some oxidic copper species, the catalysts are all under-exchanged, which we defined as less than 2 Cu per Si for silicoaluminophosphates such as SAPO-34. The amount of oxidic copper on Cu/SAPO-34 with a loading of ~1.60 wt % Cu decreased significantly after high temperature treatment at 750 °C, compared to a sample treated at only 550 °C. On the basis of conclusions drawn in other studies, we can attribute this to the migration of external CuO clusters to the ion exchange positions in the pores of the CHA structure [49–51]. Interestingly, at the lower copper loading of 1.20 wt %, we found the amount of CuO observable by UV-vis to be negligible, independently of the calcination temperature. This observation is in agreement with the colour of the 1.2 wt % Cu sample, which was blue, also independently of temperature. The 1.49 wt % sample however, was grey when CuO was present, and blue again after calcination at 750 °C caused the Cu ions to migrate from the surface into the pores. In fact, all samples below 1.49 wt % Cu maintained their blue colour independently of the calcination temperature, while those with higher Cu loadings were grey after 550 °C-treatment and blue after 750 °C treatment. We therefore postulate the following: CuO species are formed on the catalyst surface in significant numbers only when using higher copper nitrate concentrations during ion-exchange. At lower loadings, the exchange positions are occupied by Cu^{2+} ions. Then, at higher copper nitrate concentrations, the above-mentioned CuO-type species populate the catalyst surface. Only upon high-temperature treatment do these species disappear, as the Cu ions migrate from the surface into the exchange sites.

The SCR reaction occurs preferentially on the Cu species in ion-exchange positions. The copper oxide particles have little impact on the SCR activity, other than providing more CuO sites for the competitive NH_3 oxidation if the catalyst is not treated at 750 °C. For the highest copper nitrate concentration used in this study (0.8 M), we speculated that some of the formed copper particles remain even after high temperature calcination, and that these particles are probably large compared to the CuO particles on the samples with smaller loadings. This hypothesis could explain the levelling off of CuO and Cu(II) as seen by UV-vis, though while some such clusters were seen with TEM/EDS, it is difficult to prove that the samples with smaller Cu loadings contain fewer of them. Ammonia storage TPD experiments showed that NH_3 adsorbs on strong and weak Brønsted and Lewis sites, and it seems that storage is more significant on Lewis sites, since it increases with copper loading. NH_3 also adsorbs on oxidic copper species and binds to them more strongly than to the Lewis sites in exchange positions. On the basis of the single peak in H_2 -TPR and in analogy with a previous finding for Cu/SSZ-13 [19], we suggest that the ion exchange positions occupied by copper ions in all our samples are those located in the 6-membered rings of the SAPO-34 chabazite structure.

SCR, NO oxidation and NH_3 oxidation activities clearly increase with copper loading (especially below 2.6 wt % Cu) and this is in line with increasing ammonia storage on both Lewis sites and oxidic copper sites. Under standard SCR conditions, the N_2O formation has two maxima (Figure 6c). The low-temperature peak has previously been attributed to the decomposition of NH_3 -NO species (possibly precursors to ammonium nitrates) on copper [42], and it has been suggested that the high-temperature peak is the result of a different mechanistic pathway, perhaps involving a different active site [41]. Twin-peaks behaviour is also seen with N_2O production during fast SCR, although in this case the low-temperature peak is much larger and likely results from ammonium nitrate decomposition [38]. This fast SCR, low-temperature N_2O formation decreases with copper loading (Figure 10). At high temperature, the opposite trend is observed: N_2O increases with Cu content up to 1.78 wt % (Figure 9b). The result at high temperature is in agreement with results for Cu/BEA, while at low temperature more N_2O was formed over Cu/BEA with higher Cu loadings [46]. The differing behaviour of the two peaks further supports the suggestion of two different sites or

mechanisms of N_2O formation over Cu/SAPO-34. Interestingly, the N_2O maxima during standard SCR both follow the same, increasing trend with Cu loading. Therefore, the formation of NH_3 -NO species on Cu/SAPO-34 under standard SCR conditions occurs by a different pathway than the N_2O formation during fast SCR. The high-temperature N_2O formation under both reaction conditions (and the low-temperature standard SCR N_2O) presumably occurs on the isolated Cu^{2+} sites that are also the main active sites for the SCR reaction, since they follow the same, increasing trend in function of copper loading. However, it appears that for the fast SCR, especially at low temperatures, the Brønsted sites also play a significant role. Indeed, the low-temperature N_2O formation during fast SCR decreases with copper content, and since this process can potentially be attributed to decomposition of ammonium nitrates, it follows that one possible interpretation is that Brønsted acid sites in SAPO-34 may be more prone to ammonium nitrate formation than copper sites. While NO_x conversion increases with copper content even for low-temperature fast SCR, the conversion over H/SAPO-34 is considerable (when compared to that obtained over H/SAPO-34 during standard SCR). We therefore suggest that the SAPO-34 structure has a strong affinity for fast SCR and N_2O formation. Since this affinity is not observed for standard SCR conditions, one may conjecture that it could be connected to NO_2 adsorbing/reacting with particular ease on Brønsted sites in SAPO-34.

4. Materials and Methods

4.1. Catalyst Preparation

Five batches of SAPO-34 were prepared and then used to produce seven batches of Cu/SAPO-34 with different copper loadings (1.13, 1.20, 1.49, 1.60, 1.75, 1.78 and 2.60 wt %). Each batch of SAPO-34 was prepared by hydrothermal synthesis from a gel with the following molar composition: Al_2O_3 : 1.06 P_2O_5 : 1.08 SiO_2 : 2.09 morpholine: 66 deionized H_2O . Pseudoboehmite (Pural SB-1, Sasol Germany GmbH, Anckelmannsplatz 1, 20537 Hamburg, Germany), H_3PO_4 (Merck, Frösundaviks Allé 1, SE-169 70 Solna, Sweden) and colloidal silica (Ludox AS-40, Aldrich, Solkraftsvägen 14C, 135 70 Stockholm, Sweden) were used as the aluminium, silicon and phosphorus sources, respectively and morpholine (Sigma-Aldrich) was the structure directing agent (SDA). Initially, H_3PO_4 was dissolved by stirring in the water for 15 min and then the pseudoboehmite was added slowly over 2 h, under continuous agitation. Stirring was then continued for another 12 h, until a uniform gel was obtained. In the next step, a second solution of colloidal silica and morpholine was prepared, which was then slowly added to the first solution over 1 h and under constant stirring. The resulting slurry was stirred for another 7 h and then aged for 24 h at room temperature without stirring. For the crystallization process, the mixture was transferred to a Teflon-lined stainless steel autoclave and heated for 72 h at 200 °C, under autogenic pressure. After crystallization, the product was left to cool to room temperature, and the solid part was then washed seven times with deionized water and filtered by centrifugation. The end product was ground to a fine powder and calcined in air at 560 °C for 6 h.

The resulting batches of SAPO-34 powder were each twice subjected to ion exchange with a 5.4 M solution of NH_4NO_3 (Sigma-Aldrich, Solkraftsvägen 14C, 135 70 Stockholm, Sweden). Per 10 g of SAPO-34, 70 mL NH_4NO_3 5.4 M were used. The SAPO-34 powder was added spoon by spoon into the stirring NH_4NO_3 solution, which caused the pH to decrease. The solution was therefore continuously buffered with 2 M NH_4OH (NH_4OH solution obtained by mixing an appropriate amount of 28% w/w NH_4OH with deionised water) so as to maintain the pH in the range 3.0–3.5 as far as possible. Thereafter the solution was heated to 80 °C, which tends to decrease the pH. Buffering was therefore continued during the heating process. Then the solution was kept stirring at 80 °C for 1 h while buffering with NH_4OH if necessary to keep the pH within the desired range. The solution was then cooled to room temperature, decanted, and the solid washed with deionized water seven times and separated from the washing water by centrifugation until the pH of the washing water was approximately 7. After each of these ion exchanges, the powder was dried for at least 12 h at 90–100 °C. A third ion-exchange with a solution of $Cu(NO_3)_2$ (Alfa Aesar, Haverhill, MA, USA) was then carried out. The concentrations of the solutions ranged between 0.05 M and 0.8 M so as to achieve the different copper loadings shown in Table 1. The relative quantity used was 4 mL of $Cu(NO_3)_2$ solution

per g of $\text{NH}_4/\text{SAPO-34}$ powder. Then, the stirring solution was heated to 70 °C. Again, the pH decreased with the increase in temperature, but the extent of the decrease depended on the molarity of the copper nitrate solution. After heating, the pH of the 0.05 and 0.2 M solutions was not adjusted as its value was clearly above 3.0. In the case of 0.4 M, the pH of the solution was adjusted to 3.0–3.5 with NH_4OH . For the 0.6 M solution, no pH adjustment was done, although the pH was around 2.6. The 0.8 M solution was adjusted to pH = 2.6. Then, the $\text{NH}_4/\text{SAPO-34}$ powder was added spoon by spoon to the stirring solution and drops of NH_4OH were added to prevent the pH from exiting the desired range of 2.6–3.5. Once all the powder had been added, stirring at 70 °C was continued for 1 h. After the exchange, the powder was cooled, washed, filtered and dried as described above. Finally, it was calcined in air at 550 °C for 3 h and a second time at 750 °C for 2 h. The only exceptions were the batches with Cu loading of 1.27 and 1.49 wt %, which were calcined only at 550 °C. A batch of H/SAPO-34 was also prepared by following the calcination procedure described above directly after the second exchange with ammonium nitrate. The synthesis conditions of all catalysts are summarised in Table 1.

For the activity experiments, approximately 750 mg of each Cu/SAPO-34 powder was coated on monoliths cut from commercial honeycomb cordierite (length: 20 mm, diameter: 21 mm, cell density: 400 cpsi). The coating of the catalysts was preceded by coating of an alumina layer (Disperal D, Sasol), in order to increase the attachment of the SAPO-34 layer. In both instances, the impregnation was performed by repeated dipping in a slurry consisting of 95% liquid phase (equal parts deionized water and ethanol) and 5% solid phase. The solid phase consisted of 95% Cu/SAPO-34 and 5% boehmite (Disperal D). After each dipping, excess slurry was blown away and the monolith dried for 3 min at 90 °C. When the desired washcoat mass had been obtained, the monolith was calcined in air at 750 °C for 2 h. Further details on catalyst and monolith preparation are available in previous publications [38,52].

4.2. Activity and Selectivity Measurements

In this study, all the activity experiments are flow reactor experiments, where the monolith was wrapped in quartz wool to prevent slip and then inserted in a horizontal quartz reactor tube approximately 800 mm long and with an internal diameter of 22 mm. The reactive gas mixture at the inlet to the reactor (Ar as balance, NH_3 , NO and/or water vapour), was regulated using Bronkhorst massflow controllers and water vapour was produced by a controlled evaporation and mixing system (CEM, Bronkhorst, Lunet 10c, 3905 NW Veenendaal, The Netherlands). The fractions of the product gases NH_3 , NO, NO_2 , N_2O and H_2O were measured at the outlet of the reactor by a MKS™ multigas 2030 Fourier transform infrared (FTIR) spectrometer. The reactor temperature was controlled by a heating unit consisting of a Eurotherm controller, a heating coil placed around the reactor tube, and a power supply. Additionally, the reactor tube was wrapped in insulation material in order to maintain the temperature. Catalyst and gas temperature during the activity experiments were measured by two K-type thermocouples located inside a central channel of the monolith and 10 mm upstream of the monolith, respectively. All lines upstream and downstream of the reactor were heated to 150 or 200 °C to prevent condensation of water vapour. The system was operated at a total flow rate of 3500 mL/min, corresponding to a gas hourly space velocity (GHSV) of 30,330 h^{-1} , on the basis of the monolith volume. Prior to the first experiment, each monolith was degreased with 4-h-long exposure to 400 ppm NH_3 , 400 ppm NO, 8% O_2 and 5% H_2O at 700 °C to ensure stable activity. Before each experiment, the catalyst surface was cleaned for 20 min with 8% O_2 at 600 °C. For each catalyst, NH_3 oxidation, NO oxidation, standard SCR and fast SCR tests were carried out with stepwise increasing temperature. The durations of the isothermal steps were different: 40 min for NH_3 oxidation at 150 °C and 30 min for all other temperatures, 20 min for all NO oxidation steps, 1 h for SCR at 150 °C and 30 min for all other temperature steps. Fast SCR steps lasted 1 h if between 150 and 350 °C and 30 min if at temperatures above 400 °C. All of the above-mentioned experiments were performed with argon as a carrier gas, and in presence of 5% H_2O . NH_3 and NO were dosed at 400 ppm and O_2 at 8% where appropriate. Only during the fast SCR experiments were NO and NO_2 dosed at 200 ppm. At each temperature step, steady state NO_x and NH_3 conversions were calculated.

NH₃-adsorption-TPD tests were also carried out for each catalyst, with an adsorption period of 2 h under 400 ppm NH₃ and 5% H₂O. The adsorption was followed by a 45-min purge, and a temperature ramp of 10 °C/min, both under argon and 5% H₂O.

4.3. Catalyst Characterisation

The synthesised catalysts were characterized using N₂ adsorption, X-ray diffraction (XRD), UV-vis spectroscopy, H₂-temperature programmed reduction (H₂-TPR), energy-dispersive X-ray spectroscopy/transmission electron microscopy (EDS/TEM) and inductively-coupled plasma sector field mass spectrometry (ICP-SFMS). ICP-SFMS was used to determine the elemental composition of the catalysts before the experiments, and was carried out by ALS Scandinavia AB. Details on H₂-TPR and EDS/TEM are given in the Supplementary Materials. Nitrogen adsorption-desorption at 77 K for Brunauer-Emmett-Teller (BET) measurements and t-plot pore volume measurements was performed using a Tristar 3000 (Micromeritics, Avantis Science Park, Rutherford 108, D-52072 Aachen, Germany) instrument. Prior to the measurement, the samples were outgassed under vacuum at 220 °C for 3 h. The X-ray diffractograms were obtained using a Bruker AXS D8 advance operating at 40 kV and 40 mA with nickel-filtered Cu K α radiation ($\lambda = 1.5418$ Å) in the range $5^\circ < 2\theta < 40^\circ$ with a step size of 0.028°. UV-vis spectroscopy was carried out using a Carry 5000 UV-Vis NIR spectrophotometer. All samples were heat-treated at their calcination temperature (either 550 or 750 °C) 24 h prior to acquisition of the UV-vis spectra.

5. Conclusions

A procedure for liquid-ion exchange of SAPO-34 with Cu was developed, since it has been shown in literature that liquid-ion-exchange of SAPO-34 is much more complex compared to regular zeolites. Thus, five under-exchanged Cu/SAPO-34 catalysts and H/SAPO-34 were synthesised. Copper loadings ranged between 1.13 and 2.60 wt % Cu, corresponding to a degree of ion exchange between 21 and 39% (calculated as 2 Cu/Si). Samples of SAPO-34 exchanged with copper nitrate solutions of molarity above 0.2 M were shown to contain significantly more oxidic copper when calcined at 550 °C than 750 °C. We propose that these oxidic copper species migrate from the surface into the chabazite structure's pores upon treatment at 750 °C. Samples of SAPO-34 exchanged at molarities of 0.2 M or lower did not contain large amounts of copper oxides and were thus not significantly impacted by higher-temperature calcination at 750 °C.

NH₃-TPD experiments showed that NH₃ adsorbs on Brønsted sites and copper sites, and also binds particularly strongly to oxidic copper sites. The overall trend of ammonia storage, SCR, NH₃ oxidation and NO oxidation activity with copper content was increasing. The SCR occurs on copper sites located in the 6-membered rings of the SAPO-34 structure (little, if any Cu occupies the large cages in these samples, given the low levels of ion exchange). Ammonia and NO oxidation also occur on oxidic copper species situated on the outer surface of the SAPO-34 structure. In addition to being active over a large temperature window, the synthesised Cu/SAPO-34 catalysts are also highly selective towards N₂ formation, during both SCR and NH₃ oxidation reactions. Larger amounts of N₂O are however formed under fast SCR conditions, with low and high-temperature maxima. Interestingly the two peaks follow differing trends with copper loading, and we suggest that different mechanistic pathways or active sites may be in play. For fast SCR conditions, we proposed that the low-temperature process may well take place mainly on Brønsted acid sites, as we showed that less N₂O is formed when increasing the copper loading. The fast SCR itself is also closely connected with Brønsted sites, as demonstrated by the considerable activity of H/SAPO-34. Higher-temperature formation of N₂O probably occurs on the same sites as the SCR reaction, given that both follow the same trend with copper content. Another interesting aspect is that the N₂O production at low temperatures for standard SCR increases with Cu loading (although it should be mentioned that the N₂O production is only between 0–2 ppm, making clear conclusions difficult), which is the opposite result compared to the fast SCR case. Thus, our data indicates that the N₂O formation at low temperature over Cu/SAPO-34 materials occurs predominately over copper sites in standard SCR conditions, and on Brønsted acid sites for fast SCR conditions.

Supplementary Materials: The following are available online at www.mdpi.com/1996-1073/10/4/489/s1.

Acknowledgments: This study was performed at the Division of Chemical Engineering and the Competence Centre for Catalysis, Chalmers University in collaboration with Cummins Inc. The financial support of Cummins Inc. and the Swedish Research Council (621-2011-4860 and 642-2014-5733) are gratefully acknowledged.

Author Contributions: K.L., K.W. and L.O. conceived and designed the experiments; K.L., F.B. and K.W. performed the experiments; K.L., F.B., K.W., A.K., K.K. and L.O. analysed the data; K.L. wrote the paper.

Conflicts of Interest: The authors declare no conflict of interest.

References

1. Forzatti, P. Present status and perspectives in de-NO_x SCR catalysis. *Appl. Catal. A Gen.* **2001**, *222*, 221–236.
2. Deutschmann, O.; Knözinger, H.; Kochloefl, K.; Turek, T. Heterogeneous Catalysis and Solid Catalysts, 1. Fundamentals. In *Ullmann's Encyclopedia of Industrial Chemistry*; Wiley-VCH Verlag GmbH & Co. KGaA: Weinheim, Germany, 2000.
3. Wang, J.; Zhao, H.; Haller, G.; Li, Y. Recent advances in the selective catalytic reduction of NO_x with NH₃ on Cu-Chabazite catalysts. *Appl. Catal. B Environ.* **2017**, *202*, 346–354.
4. Dosda, S.; Berthout, D.; Mauviot, G.; Nogue, A. Modeling of a DOC SCR-F SCR Exhaust Line for Design Optimization Taking into Account Performance Degradation due to Hydrothermal Aging. *SAE Int. J. Fuels Lubr.* **2016**, *9*, 621–632.
5. Pereira, M.V.L.; Nicolle, A.; Berthout, D. Hydrothermal aging effects on Cu-zeolite NH₃-SCR catalyst. *Catal. Today* **2015**, *258*, 424–431.
6. Fu, M.; Li, C.; Lu, P.; Qu, L.; Zhang, M.; Zhou, Y.; Yu, M.; Fang, Y. A review on selective catalytic reduction of NO_x by supported catalysts at 100–300 C—Catalysts, mechanism, kinetics. *Catal. Sci. Technol.* **2014**, *4*, 14–25.
7. Toops, T.J.; Pihl, J.A.; Partridge, W.P. Fe-Zeolite Functionality, Durability, and Deactivation Mechanisms in the Selective Catalytic Reduction (SCR) of NO_x with Ammonia. In *Urea-SCR Technology for deNO_x after Treatment of Diesel Exhausts*; Nova, I., Tronconi, E., Eds.; Springer: New York, NY, USA, 2014; pp. 97–121.
8. Niu, C.; Shi, X.; Liu, F.; Liu, K.; Xie, L.; You, Y.; He, H. High hydrothermal stability of Cu-SAPO-34 catalysts for the NH₃-SCR of NO_x. *Chem. Eng. J.* **2016**, *294*, 254–263.
9. Liu, F.; Xie, L.; Shi, X.; He, H. Emerging Applications of Environmentally Friendly Zeolites in the Selective Catalytic Reduction of Nitrogen Oxides. In *Zeolites in Sustainable Chemistry*; Springer: Berlin/Heidelberg, Germany, 2016; pp. 393–434.
10. Gao, F.; Walter, E.D.; Washton, N.M.; Szanyi, J.; Peden, C.H.F. Synthesis and Evaluation of Cu-SAPO-34 Catalysts for Ammonia Selective Catalytic Reduction. 1. Aqueous Solution Ion Exchange. *ACS Catal.* **2013**, *3*, 2083–2093.
11. Gao, F.; Walter, E.D.; Washton, N.M.; Szanyi, J.; Peden, C.H.F. Synthesis and evaluation of Cu/SAPO-34 catalysts for NH₃-SCR 2: Solid-state ion exchange and one-pot synthesis. *Appl. Catal. B Environ.* **2015**, *162*, 501–514.
12. Ma, L.; Cheng, Y.; Cavataio, G.; McCabe, R.W.; Fu, L.; Li, J. In situ DRIFTS and temperature-programmed technology study on NH₃-SCR of NO_x over Cu-SSZ-13 and Cu-SAPO-34 catalysts. *Appl. Catal. B Environ.* **2014**, *156–157*, 428–437.
13. Kwak, J.H.; Tran, D.; Szanyi, J.; Peden, C.H.F.; Lee, J.H. The Effect of Copper Loading on the Selective Catalytic Reduction of Nitric Oxide by Ammonia Over Cu-SSZ-13. *Catal. Lett.* **2012**, *142*, 295–301.
14. Dědeček, J.; Sobalik, Z.; Tvaruazkova, Z.; Kaucky, D.; Wichterlová, B. Coordination of Cu Ions in High-Silica Zeolite Matrixes. Cu⁺ Photoluminescence, IR of NO Adsorbed on Cu²⁺, and Cu²⁺ ESR Study. *J. Phys. Chem.* **1995**, *99*, 16327–16337.
15. Gao, F.; Walter, E.D.; Karp, E.M.; Luo, J.; Tonkyn, R.G.; Kwak, J.H.; Szanyi, J.; Peden, C.H.F. Structure-activity relationships in NH₃-SCR over Cu-SSZ-13 as probed by reaction kinetics and EPR studies. *J. Catal.* **2013**, *300*, 20–29.
16. Mihai, O.; Widyastuti, C.R.; Andonova, S.; Kamasamudram, K.; Li, J.; Joshi, S.Y.; Currier, N.W.; Yezerets, A.; Olsson, L. The effect of Cu-loading on different reactions involved in NH₃-SCR over Cu-BEA catalysts. *J. Catal.* **2014**, *311*, 170–181.
17. Moden, B.; Donohue, J.M.; Cormier, W.E.; Li, H.X. Effect of Cu-loading and structure on the activity of Cu-exchanged zeolites for NH₃-SCR. In *Studies in Surface Science and Catalysis*; Antoine Gédéon, P.M., Florence, B., Eds.; Elsevier: Amsterdam, The Netherlands, 2008; Volume 174, Part B, pp. 1219–1222.

18. Shelef, M. Selective Catalytic Reduction of NO_x with N-Free Reductants. *Chem. Rev.* **1995**, *95*, 209–225.
19. Kwak, J.H.; Zhu, H.; Lee, J.H.; Peden, C.H.F.; Szanyi, J. Two different cationic positions in Cu-SSZ-13? *Chem. Commun.* **2012**, *48*, 4758–4760.
20. Wang, D.; Zhang, L.; Li, J.; Kamasamudram, K.; Epling, W.S. NH₃-SCR over Cu/SAPO-34—Zeolite acidity and Cu structure changes as a function of Cu loading. *Catal. Today* **2014**, *231*, 64–74.
21. Xue, J.; Wang, X.; Qi, G.; Wang, J.; Shen, M.; Li, W. Characterization of copper species over Cu/SAPO-34 in selective catalytic reduction of NO_x with ammonia: Relationships between active Cu sites and de-NO_x performance at low temperature. *J. Catal.* **2013**, *297*, 56–64.
22. Fan, S.; Xue, J.; Yu, T.; Fan, D.; Hao, T.; Shen, M.; Li, W. The effect of synthesis methods on Cu species and active sites over Cu/SAPO-34 for NH₃-SCR reaction. *Catal. Sci. Technol.* **2013**, *3*, 2357–2364.
23. Wang, L.; Li, W.; Qi, G.; Weng, D. Location and nature of Cu species in Cu/SAPO-34 for selective catalytic reduction of NO with NH₃. *J. Catal.* **2012**, *289*, 21–29.
24. Thommes, M. Textural Characterization of Zeolites and Ordered Mesoporous Materials. In *Introduction to Zeolite Molecular Sieves*, 3rd ed.; Čejka, J., van Bekkum, H., Corma, A., Schüth, F., Eds.; Elsevier: Amsterdam, The Netherlands, 2007; Volume 168.
25. Fickel, D.W.; D'Addio, E.; Lauterbach, J.A.; Lobo, R.F. The ammonia selective catalytic reduction activity of copper-exchanged small-pore zeolites. *Appl. Catal. B Environ.* **2011**, *102*, 441–448.
26. Kwak, J.H.; Tonkyn, R.G.; Kim, D.H.; Szanyi, J.; Peden, C.H.F. Excellent activity and selectivity of Cu-SSZ-13 in the selective catalytic reduction of NO_x with NH₃. *J. Catal.* **2010**, *275*, 187–190.
27. Park, J.-H.; Park, H.J.; Baik, J.H.; Nam, I.-S.; Shin, C.-H.; Lee, J.-H.; Cho, B.K.; Oh, S.H. Hydrothermal stability of CuZSM5 catalyst in reducing NO by NH₃ for the urea selective catalytic reduction process. *J. Catal.* **2006**, *240*, 47–57.
28. Ma, L.; Cheng, Y.; Cavataio, G.; McCabe, R.W.; Fu, L.; Li, J. Characterization of commercial Cu-SSZ-13 and Cu-SAPO-34 catalysts with hydrothermal treatment for NH₃-SCR of NO_x in diesel exhaust. *Chem. Eng. J.* **2013**, *225*, 323–330.
29. Bates, S.A.; Verma, A.A.; Paolucci, C.; Parekh, A.A.; Anggara, T.; Yezerets, A.; Schneider, W.F.; Miller, J.T.; Delgass, W.N.; Ribeiro, F.H. Identification of the active Cu site in standard selective catalytic reduction with ammonia on Cu-SSZ-13. *J. Catal.* **2014**, *312*, 87–97.
30. Dědeček, J.; Wichterlová, B. Role of Hydrated Cu Ion Complexes and Aluminum Distribution in the Framework on the Cu Ion Siting in ZSM-5. *J. Phys. Chem. B* **1997**, *101*, 10233–10240.
31. Wilken, N.; Nedyalkova, R.; Kamasamudram, K.; Li, J.; Currier, N.; Vedaiyan, R.; Yezerets, A.; Olsson, L. Investigation of the Effect of Accelerated Hydrothermal Aging on the Cu Sites in a Cu-BEA Catalyst for NH₃-SCR Applications. *Top. Catal.* **2013**, *56*, 317–322.
32. Kortüm, G. *Reflectance Spectroscopy: Principles, Methods, Applications*; Springer-Verlag: New York, NY, USA, 1969.
33. Wang, J.; Yu, T.; Wang, X.; Qi, G.; Xue, J.; Shen, M.; Li, W. The influence of silicon on the catalytic properties of Cu/SAPO-34 for NO_x reduction by ammonia-SCR. *Appl. Catal. B Environ.* **2012**, *127*, 137–147.
34. Yu, T.; Fan, D.; Hao, T.; Wang, J.; Shen, M.; Li, W. The effect of various templates on the NH₃-SCR activities over Cu/SAPO-34 catalysts. *Chem. Eng. J.* **2014**, *243*, 159–168.
35. Briend, M.; Vomscheid, R.; Peltre, M.J.; Man, P.P.; Barthomeuf, D. Influence of the Choice of the Template on the Short- and Long-Term Stability of SAPO-34 Zeolite. *J. Phys. Chem.* **1995**, *99*, 8270–8276.
36. Prakash, A.; Unnikrishnan, S. Synthesis of SAPO-34: High silicon incorporation in the presence of morpholine as template. *J. Chem. Soc. Faraday Trans.* **1994**, *90*, 2291–2296.
37. Weitkamp, J. Zeolites and catalysis. *Solid State Ion.* **2000**, *131*, 175–188.
38. Leistner, K.; Mihai, O.; Wijayanti, K.; Kumar, A.; Kamasamudram, K.; Currier, N.W.; Yezerets, A.; Olsson, L. Comparison of Cu/BEA, Cu/SSZ-13 and Cu/SAPO-34 for ammonia-SCR reactions. *Catal. Today* **2015**, *258*, 49–55.
39. Yu, T.; Wang, J.; Shen, M.; Li, W. NH₃-SCR over Cu/SAPO-34 catalysts with various acid contents and low Cu loading. *Catal. Sci. Technol.* **2013**, *3*, 3234–3241.
40. Devadas, M.; Kröcher, O.; Elsener, M.; Wokaun, A.; Söger, N.; Pfeifer, M.; Demel, Y.; Mussmann, L. Influence of NO₂ on the selective catalytic reduction of NO with ammonia over Fe-ZSM5. *Appl. Catal. B Environ.* **2006**, *67*, 187–196.

41. Wilken, N.; Wijayanti, K.; Kamasamudram, K.; Currier, N.W.; Vedaiyan, R.; Yezerets, A.; Olsson, L. Mechanistic investigation of hydrothermal aging of Cu-Beta for ammonia SCR. *Appl. Catal. B Environ.* **2012**, *111–112*, 58–66.
42. Olsson, L.; Wijayanti, K.; Leistner, K.; Kumar, A.; Joshi, S.; Kamasamudram, K.; Currier, N.W.; Yezerets, A. A multi-site kinetic model for NH₃-SCR over Cu/SSZ-13. *Appl. Catal. B Environ.* **2015**, *174–175*, 212.
43. Grossale, A.; Nova, I.; Tronconi, E.; Chatterjee, D.; Weibel, M. The chemistry of the NO/NO₂-NH₃ “fast” SCR reaction over Fe-ZSM5 investigated by transient reaction analysis. *J. Catal.* **2008**, *256*, 312–322.
44. Forzatti, P.; Lietti, L.; Nova, I.; Tronconi, E. Diesel NO_x aftertreatment catalytic technologies: Analogies in LNT and SCR catalytic chemistry. *Catal. Today* **2010**, *151*, 202–211.
45. Gao, F.; Wang, Y.; Kollár, M.; Washton, N.M.; Szanyi, J.; Peden, C.H. A comparative kinetics study between Cu/SSZ-13 and Fe/SSZ-13 SCR catalysts. *Catal. Today* **2015**, *258*, 347–358.
46. Mihai, O.; Widyastuti, C.; Kumar, A.; Li, J.; Joshi, S.; Kamasamudram, K.; Currier, N.; Yezerets, A.; Olsson, L. The Effect of NO₂/NO_x Feed Ratio on the NH₃-SCR System Over Cu-Zeolites with Varying Copper Loading. *Catal. Lett.* **2014**, *144*, 70–80.
47. Eng, J.; Bartholomew, C.H. Kinetic and Mechanistic Study of NO_x Reduction by NH₃ over H-Form Zeolites. *J. Catal.* **1997**, *171*, 27–44.
48. Schwidder, M.; Heikens, S.; De Toni, A.; Geisler, S.; Berndt, M.; Brückner, A.; Grünert, W. The role of NO₂ in the selective catalytic reduction of nitrogen oxides over Fe-ZSM-5 catalysts: Active sites for the conversion of NO and of NO/NO₂ mixtures. *J. Catal.* **2008**, *259*, 96–103.
49. Wang, J.; Huang, Y.; Yu, T.; Zhu, S.; Shen, M.; Li, W.; Wang, J. The migration of Cu species over Cu-SAPO-34 and its effect on NH₃ oxidation at high temperature. *Catal. Sci. Technol.* **2014**, *4*, 3004–3012.
50. Wang, L.; Gaudet, J.R.; Li, W.; Weng, D. Migration of Cu species in Cu/SAPO-34 during hydrothermal aging. *J. Catal.* **2013**, *306*, 68–77.
51. Vennestrøm, P.N.R.; Katerinopoulou, A.; Tiruvalam, R.R.; Kustov, A.; Moses, P.G.; Concepcion, P.; Corma, A. Migration of Cu Ions in SAPO-34 and Its Impact on Selective Catalytic Reduction of NO_x with NH₃. *ACS Catal.* **2013**, *3*, 2158–2161.
52. Leistner, K.; Olsson, L. Deactivation of Cu/SAPO-34 during low-temperature NH₃-SCR. *Appl. Catal. B Environ.* **2015**, *165*, 192–199.



© 2017 by the authors. Licensee MDPI, Basel, Switzerland. This article is an open access article distributed under the terms and conditions of the Creative Commons Attribution (CC BY) license (<http://creativecommons.org/licenses/by/4.0/>).